Application of the CESE Method to Detonation with Realistic Finite-Rate Chemistry

Kyoung-Su Im[1], S.-T. John Yu[2], Chang-Kee Kim,[3]

Wayne State University, Detroit, MI48202

Sin-Chung Chang[4], and Philip C.E. Jorgenson[5]

NASA Glenn Research Center, Cleveland, OH44135

Abstract

In the present paper, we report high fidelity simulation of detonation initiated by reflected shock waves, propagating in premixed hydrogen/oxygen gas mixtures. Comprehensive model equations are solved by the Space-Time Conservation Element and Solution Element (CESE) method, including correctly derived Jacobian matrix and source term matrix, and comprehensive thermodynamics relations. Chemical reactions are modeled by two sets of reduced kinetics proposed by Oran et al. [14] and Youngster and Radhakrishnan [12] with nine specie/twenty-four reaction steps, and nine species/nineteen reaction steps, respectively. In the setting of the CESE method, stiff source terms in species equations due to chemical reactions are treated based on a unique space-time volumetric integration. Sub-time-step integrations are applied to resolve the chemical reaction time scales. The present approach is validated by favorable comparison between the present results and the equilibrium calculations by using the CEA program [10], and comparisons between the present approach and previous results by Oran et al. and Youngster and Radhakrishnan.

1. Introduction

In a series of papers [2,3,4,5,7,9], we showed that the CESE method is highly accurate and very efficient for calculating traveling detonations with a one-step irreversible chemistry model. Progresses in extension to realistic finite-rate models by using the CESE method has been reported in [7,8,15]. Previously, other CFD methods have been applied to detonations with realistic finite rate chemistry models, e.g., [12,13,14].

In the present paper, we revisit the application of the CESE method to detonation with realistic finite rate chemistry. The specific goal of the present paper is twofold: (1) numerical approach here is validated through comparisons with the previously published results and the thermodynamic equilibrium results, and (2) the thermodynamics model has been extended to include the calculations of equilibrium constants for deducing the reverse reaction rates. For completeness, all theoretical model equations and their numerical treatment are briefly reviewed in the present paper.

The CESE method [1-4] is distinguished by the simplicity of its conceptual basis — flux conservation in space and time. This method has been extensively illustrated in the context of conservation laws in fluid dynamics. The CESE method emphasizes space-time flux conservation based on a novel space-time integral equation, which treats space and time as one entity. The present integral equation is different from the transport theory used in traditional finite volume methods. The unified treatment of space and time in the present method cannot be overemphasized. To integrate the space-time equation, the concept of the

[1] Research Assistant Professor, AIAA member, Email: ksim@fluid.eng.wayne.edu
[2] Associate Professor, AIAA member, Email: styu@me1.eng.wayne.edu
[3] Research Associate, AIAA member, Email:ckkim@fluid.eng.wayne.edu
[4] Aerospace Engineer, AIAA Member, Email: sin-chung.chang@grc.nasa.gov
[5] Aerospace Engineer, AIAA Member,

Solution Element (SE) and the Conservation Element (CE) are introduced. In an SE, flow variables are continuous and are discretized by a predetermined function. Over a CE, space-time flux conservations is imposed and contact discontinuities of flow variables are allowed.

The flow variable distribution inside an SE is not calculated by interpolation or extrapolation, i.e., no reconstruction procedure is used. Instead, spatial gradients of flow variables are treated as independent unknowns. Thus their values are not influenced by the neighboring flow variables at the same time level. This is in full compliance with the nature of initial-value problems. A leapfrog marching strategy in the space-time domain is employed, such that flow information across interfaces of neighboring SEs propagates only in one direction, i.e., toward at the future. Thus the calculation of the space-time flux is straightforward, and no Riemann solver is needed. Previously, we have reported numerous numerical results obtained by using the one-, two-, and three-dimensional CESE computer programs, including various traveling shock waves, shock/acoustics interactions, cavitations, and particle embedded turbulent flows.

In the present paper, the CESE method is further extended for chemically reacting flows with comprehensive physical modeling, including the multi-step finite-rate kinetics and thermodynamics models. Moreover, previous treatments for stiff source terms are modified to accommodate vast discrepancies of time scales between various reaction steps.

The rest of the paper is organized in the following sections. In Section 2, we present the model equations and the associated numerical treatments. The emphasis is placed on special features relevant to chemical reactions only. In section 3, we present our numerical results and the comparison with previously reported results. We then offer concluding remarks and provide cited references.

2. Theoretical Model

2.1 Governing Equations

We consider the unsteady, inviscid, and chemically reacting flow equations in one spatial dimension:

$$\frac{\partial \mathbf{Q}}{\partial t}+\frac{\partial \mathbf{E}}{\partial x}=\mathbf{S} \qquad (2.1)$$

$$\text{where, } \mathbf{Q}=\begin{pmatrix}\rho u\\ \rho E\\ \rho_1\\ \rho_2\\ \vdots\\ \rho_{\text{Ns-1}}\end{pmatrix}, \mathbf{E}=\begin{pmatrix}\rho u^2+p\\ (\rho E+p)u\\ \rho_1 u\\ \rho_2 u\\ \vdots\\ \rho_{\text{Ns-1}}u\end{pmatrix}, \mathbf{S}=\begin{pmatrix}0\\ 0\\ \dot{\omega}_1\\ \dot{\omega}_2\\ \vdots\\ \dot{\omega}_{\text{Ns-1}}\end{pmatrix} \qquad (2.2)$$

The first two equations are the momentum and energy equations, and the rest of the equation set are N_s species equations, describing the mass conservation of each gas species. In Eq. (2.2), ρ is the density of the gas mixture and

$$\rho=\sum_{i=1}^{Ns}\rho_i \qquad (2.3)$$

with ρ_i as the density of species i. u is the velocity of the gas mixture, and E is the total energy of the gas mixture per unit mass, which is defined as

$$E=e+\frac{u^2}{2} \qquad (2.4)$$

where e is the internal energy of the gas mixture per unit mass, and it is calculated based on a mass-weighted average of the internal energy per unit mass of each species e_i, i.e.,

$$e=\sum_{i=1}^{Ns}Y_i e_i \qquad (2.5)$$

Note that $Y_i=\rho_i/\rho$ is the mass fraction of species i in the gas mixture. The definitions of internal energy e and total energy E include the heat of formation of chemical species. Thus no source term exists in the energy equation.

The source terms in the species equations are due to chemical reactions. Because total mass is conserved, the summation of all source terms is null:

$$\sum_{i=1}^{Ns}\dot{\omega}_i=0 \qquad (2.6)$$

Thus, summation of all species equations recovers the original continuity equation:

$$\frac{\partial \rho}{\partial t}+\frac{\partial \rho u}{\partial x}=0 \qquad (2.7)$$

Equation (2.1) is N_s+2 equations for N_s+2 unknowns. With proper initial and boundary conditions, the equation set is well posed. However, pressure appears in the spatial flux $\boldsymbol{E}$ in both momentum and energy equations, and is not one of the unknowns. Thus an additional equation of state, e.g.,

$$p=p(\rho u,\rho E,\rho_1,\rho_2,\cdots,\rho_{Ns}) \qquad (2.8)$$

must be supplemented to close the equation set. For non-reacting flows, the calorically perfect gas equation $p = (\gamma - 1)\rho e$ is usually used, where $\gamma = C_p/C_v$ is the specific hear ratio. For reacting flows, due to the changing chemical compositions, the above desired relationship is very complex and will be illustrated in the following subsections.

2.2 Thermodynamic Model

In general, N_s+1 variables are needed to determine an equilibrium thermodynamic state of a gas mixture. If we always choose $\rho_1,\rho_2,...,\rho_{N_s}$ as variables, we could have the following equations of state,

$$\begin{aligned} p &= p(e, \rho_1, \rho_2, \ldots, \rho_{N_s}) \\ p &= p(T, \rho_1, \rho_2, \ldots, \rho_{N_s}) \\ e &= e(T, \rho_1, \rho_2, \ldots, \rho_{N_s}) \end{aligned} \qquad (2.9)$$

Note that the first equation in (2.9) is the desired relation for the well-posedness of the governing equations. Unfortunately, we cannot find an explicit form for it. The explicit form of the second equation in (2.9) is the ideal gas equation for the gas mixture, which is given by

$$p = \rho R_u T \sum_{i=1}^{N_s} \frac{Y_i}{M_i} \qquad (2.10)$$

The explicit form of the third equation in (2.9) can be obtained by substituting the definition of *e,* and the ideal gas equation for each species into the definition of h , and we obtain

$$e = h - \frac{p}{\rho} = \sum_{i=1}^{Ns} \frac{\rho_i}{\rho} h_i - \frac{p}{\rho}, \qquad (2.11a)$$

with

$$h_i = \int_{T_{ref}}^{T} C_{pi} dT + h_{fi} \qquad (2.11b)$$

The integration constant h_{fi} is the heat of formation. Note that the ideal gas equation

$$p = \rho RT \qquad (2.11c)$$

is assumed valid for the reacting gas mixture. As a result, C_{pi} in (2.11b) for $i = 1,..., Ns$ are functions of T only. A database for C_{pi} is available in [13]. Therefore, if the unknown variables ($\boldsymbol{Q}$ in Eq.(2.2)) at a certain space-time location are known, Eq. (2.11) can be used to calculate T by using an iterative procedure.

With the known T, p is readily obtained by the ideal gas equation, (2.11c). The specific heat of individual species C_{pi} appearing in Eq. (2.11) is determined by fourth order polynomials of temperature such as

$$\frac{C_{pi}}{R_u} = a_{i1} + a_{i2}T + a_{i3}T^2 + a_{i4}T^3 + a_{i5}T^4 \qquad (2.12)$$

The coefficients of these polynomials are supplied by Gordon and McBride and are valid up to a temperature range 200K to 6000K [13].

In the literatures, many researchers do not provide the kinetic data for the reverse reactions, which are needed in a comprehensive finite rate chemistry model. In this case, the equilibrium constant is used to calculate the reverse reaction rate. Thus, one needs to calculate the Gibbs energy.

In [13], additional coefficients, i.e., a_{i6} and a_{i7}, are provided such that the enthalpy and the entropy of each species, which are needed to calculate the Gibbs energy, can be obtained by the specific heat of individual species:

$$\begin{aligned} \frac{h_i}{R_u T} &= \frac{1}{R_u T}\left\{\int_{T_{ref}}^{T} C_{pi} dT + h_{fi}\right\} \\ &= a_{i1} + \frac{a_{i2}}{2}T + \frac{a_{i3}}{3}T^2 + \frac{a_{i4}}{4}T^3 + \frac{a_{i5}}{5}T^4 + \frac{a_{i6}}{T} \end{aligned} \qquad (2.13)$$

and

$$\begin{aligned} \frac{s_i}{R_u} &= \int_{T_{ref}}^{T} \frac{dh_i}{R_u T} = \int_{T_{ref}}^{T} \frac{C_{pi} dT}{R_u T} \\ &= a_{i1}\ln T + a_{i2}T + \frac{a_{i3}}{2}T^2 + \frac{a_{i4}}{3}T^3 + \frac{a_{i5}}{4}T^4 + a_{i7} \end{aligned} \qquad (2.14)$$

Based on the above equations, the Gibbs energy of each species can be obtained,

$$\begin{aligned} \frac{g_i}{R_u T} &= \frac{h_i - Ts_i}{R_u T} \\ &= a_{i1}(1 - \ln T) - \frac{a_{i2}}{2}T - \frac{a_{i3}}{6}T^2 - \frac{a_{i4}}{12}T^3 - \frac{a_{i5}}{20}T^4 + a_{i6}/T - a_{i7} \end{aligned} \qquad (2.15)$$

Thus, the Gibbs energy of reaction is calculated as the difference energy between the products and reactant species:

$$\Delta G_j = \sum_{i=1}^{N_s} \nu''_{ji} g_i - \sum_{i=1}^{N_s} \nu'_{ji} g_i, \qquad j = 1,2,\ldots,Nr \qquad (2.16)$$

The equilibrium constant for each chemical reaction can then be determined from,

$$K_{eqj} = \left(\frac{1}{R_u T}\right)^{\Delta n} \exp\left[-\Delta G_j /(R_u T)\right] \qquad (2.17)$$

where Δn is the change in the number of moles between the reactants and the products.

2.3 Jacobian Matrix of Flux Vector

The derivation of the Jacobian matrix of flux vector is not straightforward because pressure of the gas mixture exist in the flux vector, and it is a function of density, internal energy, and species composition.

By directly dealing with the flow equations in the conservative form, i.e., (2.1), one could derive all elements of the Jacobian matrix by applying the chain rule for partial derivatives. Or, as shown in [8], it is much easier to derive the Jacobian matrix of the flow equations in a non-conservative form. And, through the similarity transformation between the conservative form and the non-conservative form, one could easily obtain the complete Jacobian matrix. In both cases, derivatives of pressure with respect to density, internal energy, and mass concentration of all species are needed.

For completeness, the Jacobian matrix A is tabulated in the following:

$$A=\frac{\partial \mathbf{E}}{\partial \mathbf{Q}}=$$

$$\begin{bmatrix} 0 & 1 & 0 & 0 & \cdots & 0 \\ -u^2\left(1-\frac{p_e}{2\rho}\right)+p_\rho-\frac{e}{\rho}p_e & u\left(2-\frac{p_e}{\rho}\right) & \frac{p_e}{\rho} & p_{\rho_1} & \cdots & p_{\rho_{N-1}} \\ u\left(-H+p_\rho+\frac{u^2}{2\rho}p_e-\frac{e}{\beta}p_e\right) & H-\frac{u^2}{\rho}p_e & u\left(1+\frac{p_e}{\rho}\right) & up_{\rho_1} & \cdots & up_{\rho_{N-1}} \\ -\frac{u}{\rho}\rho_1 & \frac{\rho_1}{\rho} & 0 & u & \cdots & 0 \\ -\frac{u}{\rho}\rho_2 & \frac{\rho_2}{\rho} & 0 & 0 & \cdots & 0 \\ \vdots & \vdots & \vdots & \vdots & \cdots & \vdots \\ -\frac{u}{\rho}\rho_{N-1} & \frac{\rho_{N-1}}{\rho} & 0 & 0 & \cdots & u \end{bmatrix}$$

where, $H=e+\frac{1}{2}u^2+(p/\rho)=E+(p/\rho)$. In [8], we also formally showed that the flux vector **E** is a first-order homogeneous function of **Q**, i.e., **E**= **AQ**. We also showed that the eigenvalues of **A** are *u, ..., u*, and $u\pm a$, where *a* is the frozen speed of sound.

2.4 Chemistry Model

According to the law of mass action, the stoichiometric equation of a set of N_r elementary reactions involving N_s species can be written in the following form

$$\sum_{i=1}^{N_s}\nu_{ji}^{'}C_i \underset{K_{bj}}{\overset{K_{fj}}{\Leftrightarrow}} \sum_{i=1}^{N_s}\nu_{ji}^{''}C_i, \quad j=1,2,\ldots,N_r \qquad (2.18)$$

where $C_i=\rho_i/M_i$ is the mole concentration of species i in the gas mixture. $\nu_{ji}^{'}$ and $\nu_{ji}^{''}$ are respectively the stoichiometric coefficients of the reactants and products of species i in the jth reaction. The forward and backward reaction rate constants, K_{fj} and, K_{bj} are given by the Arrhenius form:

$$\begin{aligned} K_{f_j} &= A_{f_j}T^{B_{f_j}}\exp\left(-E_{f_j}/R_uT\right) \\ K_{b_j} &= A_{b_j}T^{B_{b_j}}\exp\left(-E_{b_j}/R_uT\right) \end{aligned} \qquad (2.19)$$

where A_f and A_b are the pre-exponential constant; E_f and E_b are the activation energies; and, R_u is the universal gas constant. In general, A_f, B_f, E_f, A_b, B_b, and E_b are given constants, associated with the finite rate model.

Measurements of reverse rate coefficients of elementary reaction steps are difficult tasks, which could lead to results with significant uncertainties. Equilibrium constants, on the other had, are based on thermodynamic calculation, and are very accurate in most conditions. Therefore, knowing the forward reaction rate, the reverse reaction rate can be calculated by

$$K_{f_j}=K_{b_j}K_{eq_j} \text{ or } K_{b_j}=K_{f_j}/K_{eq_j} \qquad (2.20)$$

where the K_{eqj} is determined from Eq.(2.17). Once the forward and reverse reaction rates are determined, the production rates of the species are obtained from the Eq. (2.21), which states that the rate of change of concentration of species i by the reaction j is given by

$$(\dot{C}_i)_j=\left(\nu_{ji}^{''}-\nu_{ji}^{'}\right)\left(K_{f_j}\prod_{l=1}^{N_s}C_l^{\nu_{jl}^{'}}-K_{b_j}\prod_{l=1}^{N_s}C_l^{\nu_{jl}^{''}}\right) \qquad (2.21)$$

The source terms, $\dot{\omega}_i$, for $i=1,2,...,N_s$, in the species equations, Eq. (2.1), are formulated in mass concentration, and they are the summation of the net rate of change of species i from all chemical reactions involved, i.e.,

$$\dot{\omega}_i=M_i\sum_{j=1}^{N_r}\left(\dot{C}_i\right)_j \qquad (2.22)$$

where M_i is the molecular weight of species

2.5 The Source Term Calculation

In the setting of the CESE method, viable treatments for stiff source terms as part of relaxing conservation laws have been developed [12]. Essentially, the contribution of the source terms to the overall flux conservation is calculated by a volumetric integration of the source term in the space-time domain.

In general, choosing a time marching step Δt based on the CFL constraint (CFL-Δt) of the convection terms is desirable for numerical efficiency. However, the chemical time scales are significantly smaller than that of the flow convection. In the past, simple implicit methods have been

adopted to calculate the source terms based on the use of the CFL-Δt to ensure numerical stability. However, this approach, although numerically robust, is not suitable for simulations of unsteady flows and/or flame ignition. A direct use of the CFL- Δt to integrate the source terms will lead to nonphysical results. Based on our experience, the combustion cannot be correctly initiated even when the physical condition ensures a vigorous ignition.

To overcome the scale differences between the convection terms and the source terms, a splitting method is developed. That is, the integration the conservation equations with stiff source terms to a new time step is divided into: (1) the space-time flux of the flow variables in the usual CESE manner, and (2) the temporal integration of the source term over a special tailored conservation element.

After each time marching step based on the CESE method, the solution of the species mass fractions are updated by using a multiple sub-time-step integration with the fixed values of ρ, u, and e. The number of the sub-time steps for the source-term integration depends on the chemistry systems employed. Typically, $\Delta t_c = \Delta t/Nc$, where $1<Nc<20$.

Figure 2.1 is a schematic for treating the source terms. First, the integration of the ODE set for chemical reactions are performed from B to E and C to F. Second, the flow solution at point *(i, j)* is calculated by the standard CESE method using the known solutions at B and C, without regard to the existence of the source terms. Finally, the solution of the species concentration are updated based on the results of the ODE integration. Usually, a simple average of the source term between E and F is used.

The integration of the ODE set is calculated by the Trapezoidal rule:

$$\Delta \mathbf{u}\Big|_B^E = \int_B^E \mathbf{S}dt = \sum_{k=1}^{Nc} \frac{\Delta t_c}{2}(\mathbf{S}^k + \mathbf{S}^{k+1}) \qquad (2.23)$$

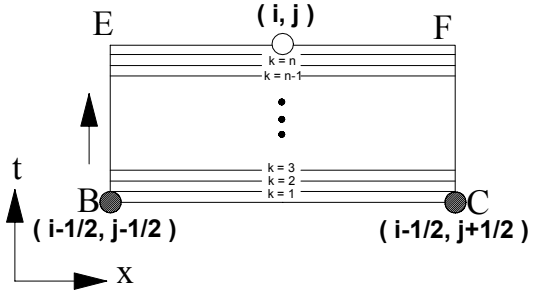

Fig. 2.1: The treatment of the temporal integration of the source term.

Note N_s species equations are considered, and Eq. (2.23) are N_s coupled equations. Let $\mathbf{u}$ be the unknown vector with densities of each species as the entries, i.e.,

$$\mathbf{u} = (\rho_1, \rho_2, \cdots, \rho_{Ns})^T$$

To treat the nonlinear source terms in (2.23), a linearization procedure is adopted to calculate the source term at the new time step, i.e.,

$$\mathbf{S}^{k+1} = \mathbf{S}^k + \left(\frac{\partial \mathbf{S}}{\partial u}\right)^k \Delta \mathbf{u}^k \qquad (2.24)$$

where $\Delta \mathbf{u}^k = \mathbf{u}^{k+1} - \mathbf{u}^k$. Since N_s species equations are considered, the matrix $\partial \mathbf{S}/\partial \mathbf{u}$ in the above equation is an $N_s \times N_s$ matrix. At each sub-time step, the discretized equation is,

$$\left[\frac{\mathbf{I}}{\Delta t_c} - \frac{1}{2}\left(\frac{\partial \mathbf{S}}{\partial u}\right)\right]^k \Delta \mathbf{u}^k = \mathbf{S}^k, \qquad \mathbf{u}^{k+1} = \mathbf{u}^k + \Delta \mathbf{u}^k \qquad (2.25)$$

2.6 The Source-Term Matrix

To integrate the stiff ODEs for chemical reactions, the source-term matrix is needed due to the linearization procedure. In general, the source-term matrix is a function of temperature and species concentration. To simplify the derivation, we assume that the source-term matrix is a function of species concentration only. Thus we have,

$$\frac{\partial \dot{C}_i}{\partial C_m} = \sum_{j=1}^{N_r} \left(\nu''_{ji} - \nu'_{ji}\right)\left(\frac{K_{f_j}\nu'_{jm}}{C_m}\prod_{l=1}^{N_s} C_l^{\nu'_{jl}} - \frac{K_{b_j}\nu''_{ji}}{C_m}\prod_{l=1}^{N_s} C_l^{\nu''_{jl}}\right), \quad i,m = 1,\ldots,N_s \qquad (2.26)$$

where C_i is the mole concentration of species i.

3. Results and Discussion

Three sets of calculations are performed to validate the present approach to calculation detonation by the CESE method: (1) simulations a well-stirred reactor, (2) simulation of detonation initiation, and (3) simulation of a C-J detonation.

3.1 Well-Stirred-Reactor Calculations

To test the thermodynamics and chemical kinetics modules, we first followed Oran et al. [] and performed simulation the ignition induction time of a hydrogen/oxygen mixture at the reflected shock temperature in a well-stirred reactor. Initially, 2 moles of H_2 are mixed with 1 moles of O_2 and 7 moles of Argon in a constant volume adiabatic vessel. The initial pressure is 1.3 atm and the initial temperature varies from 1000 to 1300K. Since no transport phenomenon is considered, the evolution of the reacting system depends only on the chemical reactions. The induction time is defined as the point at which the initial temperature increases by 20 K [14]. Figure 3.1 shows the comparison between the present results and results by Oran et al. [14]. Note that the induction time for T_i= 1034 K, marked by a star, was measured by a shock tube experiment.

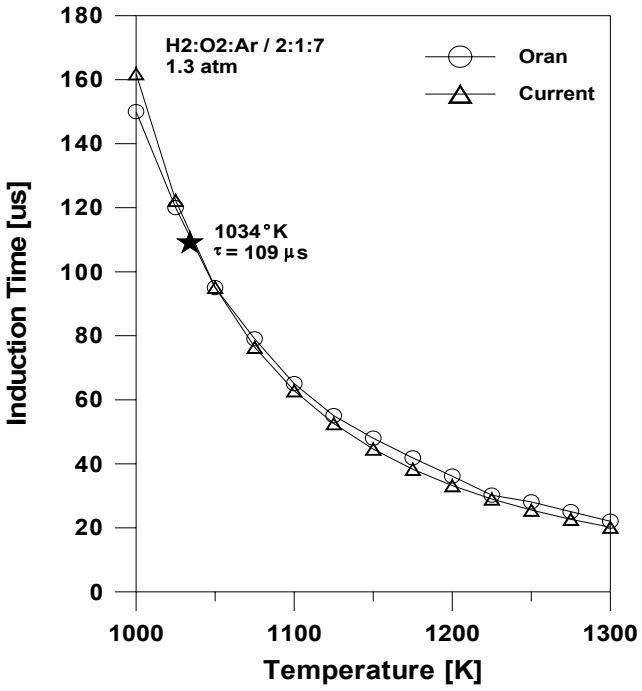

Fig. 3.1 Calculations of chemical induction time as a function of temperature.

3.2 Detonation Initiation

The detonation in the present paper is generated by a reflected shock at the closed end of a long tube as shown in Fig. 3.2. Two cases of detonation initiation were studied: (1) the strong ignition case by Oran et al. [14], and (2) a numerical testing by Yungster [12].

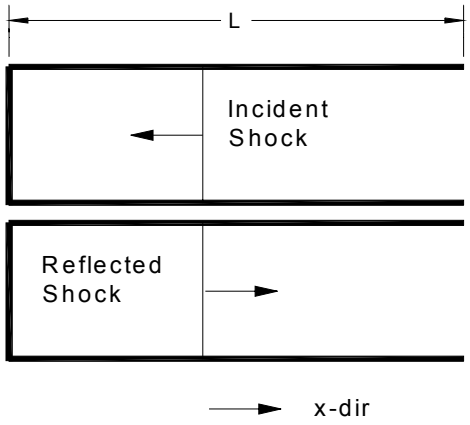

Fig. 3.2: Schematic of shock tube configuration.

Initially, the tube is filled with a mixture of $2H_2$ + O_2 + 7Ar. An incident shock wave is created which travels from right to left. When the incident shock reflects from the closed end, the detonation wave is formed by the shock heating.

In the first case, the initial pressure 0.066 atm (6687.45 Pa) and temperature 298K. The Mach number of the incident shock is 2.165. The CFL number of the calculation is about 0.44 and Δx = 0.000025 m. The total calculation length varies from 15 cm to 20 cm for the solution to reach a stable detonation. The hydrogen-oxygen-argon reaction chemistry is modeled by finite-rate kinetics with 9 species and 24 reaction steps (see Appendix), which was developed in reference [14] for the shock tube experimental and simulation.

To examine the flow evolution, the time histories of pressures and velocity at reflective wall are shown in Fig. 3.3. When the incident shock reflects from the wall, the wall pressure jumps to a high value. If the shock heating triggered chemical reactions, energy is released and the wall pressure increases further. If the reaction wave catches up with the reflected shock wave, the wall pressure reaches its maximum.

For non-reacting flows, fluid velocities behind a reflected shock are null. Due to combustion ignition, however, velocities at wall jump to about 3000 cm/s. If the reaction wave catches up with the reflected shock wave, an expansion wave is generated by the

interacting shock and reaction waves. This expansion wave continuously moves to the closed wall. As a result, the fluid velocity at wall temporally rises to certain values. Figure 3.3 shows excellent comparison between the present calculations and experimental and numerical results by Oran et al.

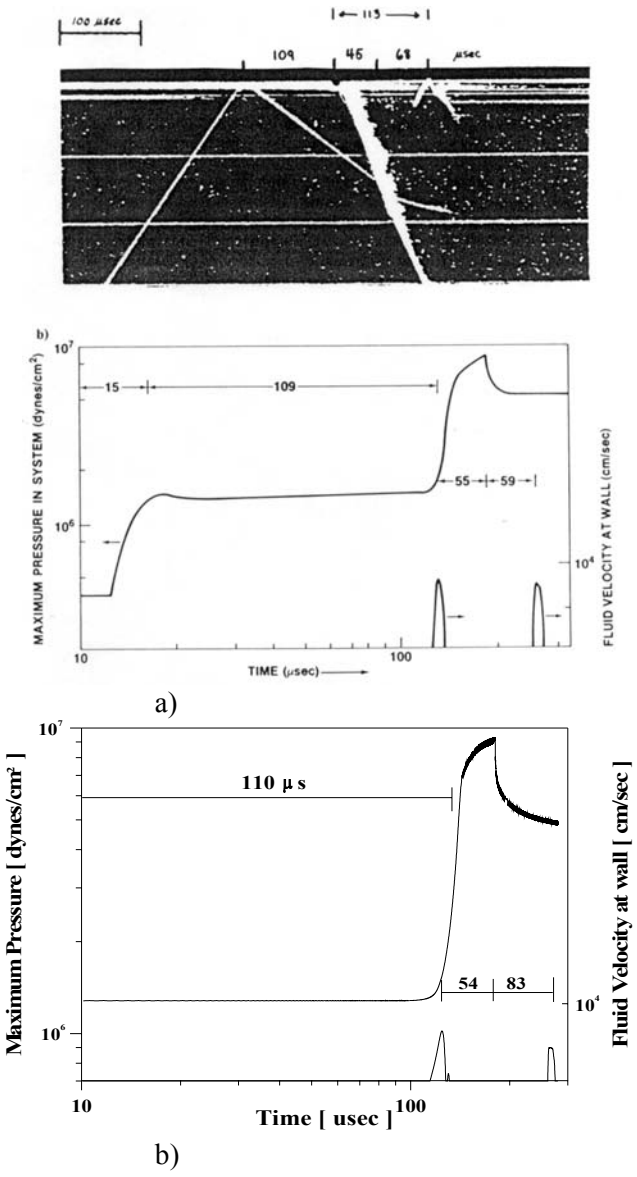

Fig. 3.3: Comparison between (a) the experimental and numerical results by Oran el al. [22] and (b) the present results for maximum pressure and fluid velocity at 1 mm from the wall.

Figure 3.4 shows temporal evolution of pressure, density, and temperature of the detonation initiation. Different stages of the detonation initiation can be clearly discerned, including ignition, development, and finally full-fledged detonation. The reaction wave created after induction time continuously evolves until it becomes a detonation wave at about 140 μs. The detonation wave catch up

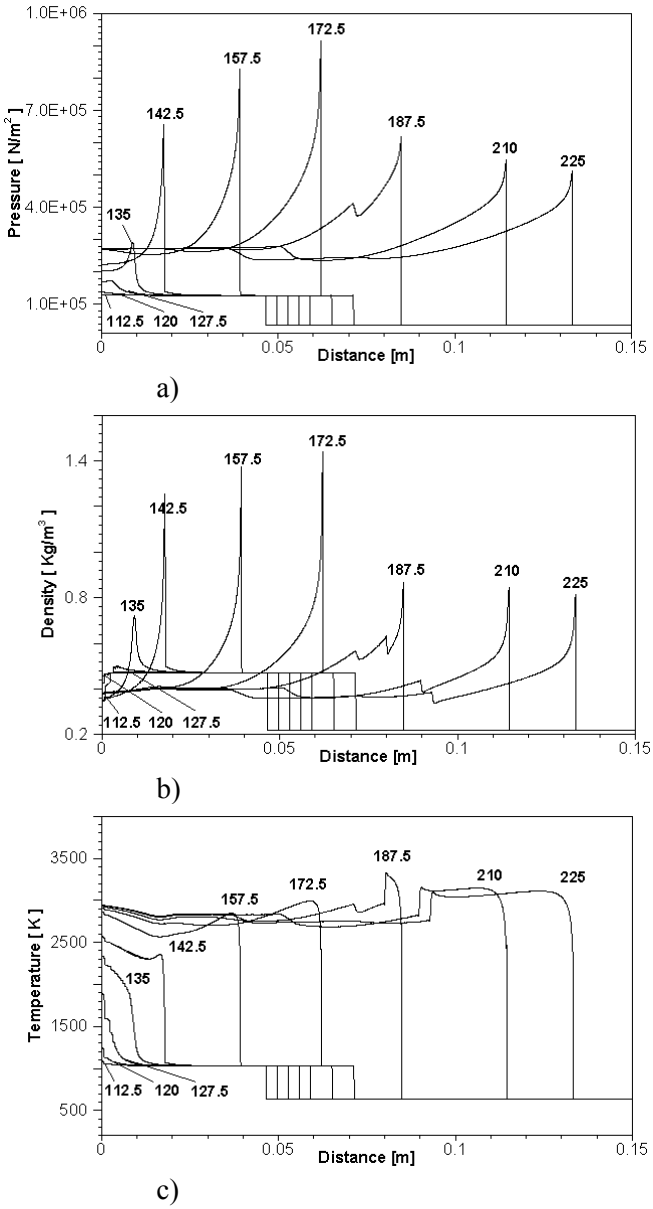

Fig. 3.4: Temporal evolution of pressure, density, and temperature of detonation ignition.

with the reflected shock wave at about 180 μs. When two waves merge, an expansion wave is generated and moves towards the wall. Eventually, the traveling detonation approaches the Chapman-Jouguet (C-J) detonation wave.

We remark that the difference in the fluid velocities before and after the collision, between the reflected shock and the detonation, causes the

formation of a contact discontinuity at 187.5 μs. The contact discontinuity moves forward at a speed slower than the detonation wave.

Figure 3.5 shows the comparison of the positions of the shock front, reaction wave, transmitted detonation, and the contact discontinuity formed as the shock merged by the reaction wave. After the reaction wave merges the reflected shock wave, it slowly decelerates relatives to laboratory coordinates due to the incoming incident reactant [14]. The merged reflected shock, which becomes the contact discontinuity, immediately accelerates for a short time due to the high velocity of the reaction wave. After this period, it will converge to a certain value.

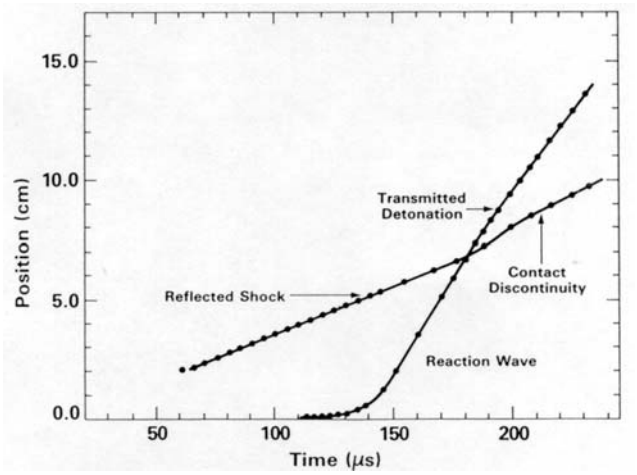

a)

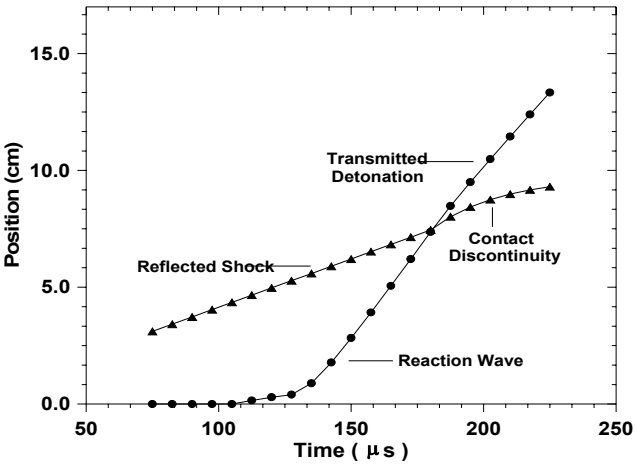

b)

Fig. 3.5: Calculated position of the reflected shock front, reaction wave, transmitted detonation, and contact discontinuity as a function of time: a) Oran's result [22], b) Current results

3.3 C-J Detonation Calculation

Finally, the post detonation flow condiitions predicted by our code are compared with the equilibrium results obtained by using the CEA program. The results are presented in Table 1. The quantities of the post detonation are well matched with that of its equilibrium in a small error percent. The detonation velocity, which is 2.5 % less than the C-J velocity, also is in good agreement with ideal case. Especially, we emphasis that the mass fraction for four main species is perfectly matched with CEA results less than 1% of error.

The second case considered in this study is one of the Yungster's conditions [12]. The same mixture as previous case at initial pressure = 50 torr, temperature = 298 K, and Mach number = 3.0 is considered.

Table 1: Result Comparison

	Current	CEA	Error %
T/T_1	4.719	4.736	0.36
ρ/ρ_1	1.610	1.732	7.04
p/p_1	7.122	7.692	7.41
D_{vel}	1575.5	1619	2.69
H_2	0.002137	0.00213	0.33
O_2	0.011817	0.01175	0.57
OH	0.01220	0.01228	0.65
H_2O	0.08399	0.08412	0.16
H	0.00051	0.00050	2.00
O	0.00349	0.00335	4.18
HO_2	0.00001	0.00001	0.00
H_2O_2	0.00000	0.00000	0.00
N2	0.88585	0.88586	0.001

Table 2 shows the results between the current study and CEA program. The detonation velocity, and mass fraction of burned mixture are well matched with CEA in less than 5% for all species. However, the post detonation properties, which are the temperature, pressure, and density ratio, show more error percent than other properties. These differences may be caused by either low resolution of mesh size or iterative calculation of the temperature by Newton method. Since the pressure is obtained by the temperature and density in simulation, the error of the pressure is proportion to the multiple of them. Therefore, the high error percent of the pressure is always obtained.

Figure 3.6 shows the discrepancy of two different chemistries in maximum pressure as a function of

time. Both chemistries are listed on the appendix. The reason for the discrepancy is unclear. It may be due to use different reaction coefficients, especially the third body coefficients. More study is required to solve this problem. In addition, the considerable error on the maximum pressure relative to the C-J value is observed. It may be due to not enough time for the stable detonation or not enough mesh size. However, the overall behavior of the strong detonation, which propagates faster than the C-J velocity and decays slowly toward the C-J condition [15], is in good with Yungster's [12].

Table 2: Result Comparison: Case 2

	Present	CEA	Error %
T/T_1	4.000	3.843	4.100
ρ/ρ_1	1.895	1.704	11.20
P/p_1	7.001	6.155	13.70
D_{vel}	1600	1620	0.200
H_2	0.00228	0.00223	2.200
O_2	0.01199	0.01205	0.498
OH	0.01401	0.01325	5.811
H_2O	0.08150	0.08236	1.044
H	0.00053	0.00054	1.886
O	0.00382	0.00370	3.225
HO_2	0.00001	0.00001	0.000
H_2O_2	0.00000	0.00000	0.000
Ar	0.88584	0.88586	0.002

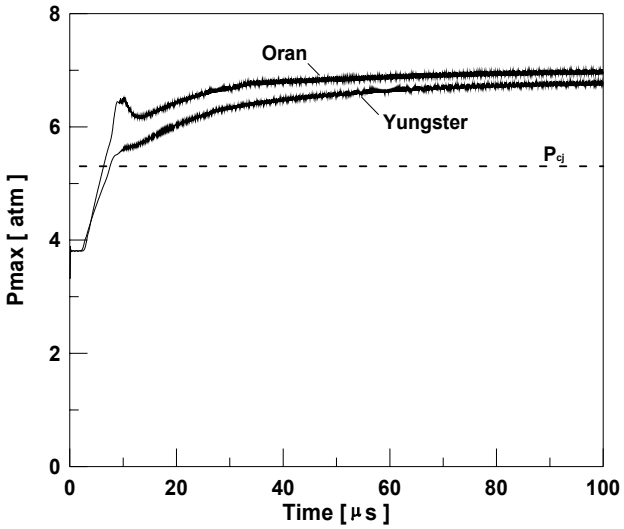

Fig. 3.6 Comparison of chemical kinetics for maximum pressure in the system.

The mass fractions of four main species are illustrated in Figure 3.7 according to traveling distance (see table 2) at time=100 μs. The mass fractions of the products and reactants are clearly distinguished before/after the detonation front.

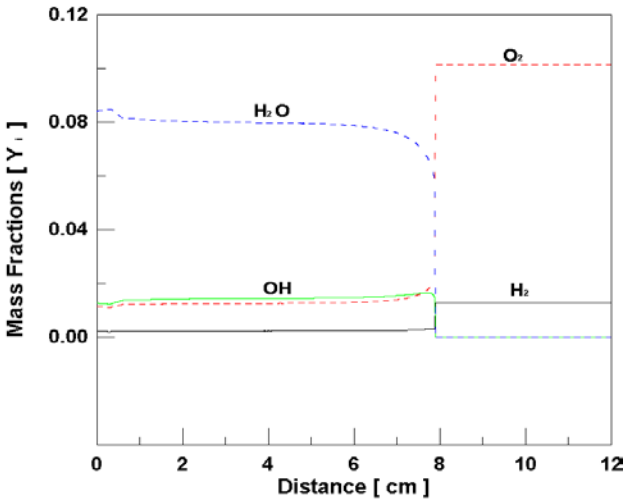

Fig. 3.7 Snapshot of species mass fraction at 100 μs.

4. Concluding Remarks

In this paper, we report the results of applying the CESE method to chemically reacting flow with realistic chemistry and thermodynamics models. The present approach is a synergy of a highly accurate CFD method, comprehensive model equations, and a robust treatment of stiff source terms. Highly accurate results are obtained. Favorable comparison with previously numerical and experimental results has been demonstrated. The present effort is a steppingstone for the further development of the CESE method for high fidelity solution of reacting flows.

5. References

1. S.C. Chang, "The method of Space-Time Conservation Element and Solution Element-A New Approach for Solving the Navier-Stokes and Euler Equations," J. Comput. Phys., 119 (1995) pp.2950324.
2. Chang
3. Wang
4. Zhang
5. S.J. Park, S.T. Yu, M.C. Lai, S.C. Chang, and P.C.E. Jorgenson, "Numerical Calculations of Two-Dimensional Unstable Detonation by Space-Time CESE Method," AIAA Paper 99-0491, the 37th Aerospace Science Meeting and Exhibit, January 1999, Reno, NV.

6. S.J. Park, S.T. Yu, M.C. Lai, S.C. Chang, and P.C.E. Jorgenson, "Direct Calculations of Stable and Unstable Detonation by the Space-Time Conservation Element and Solution Element Method," AIAA Paper 98-3212, the 34th AIAA/ASME/SAE Joint Propulsion Conference and Exhibit, July, 1998, Cleveland, OH.

7. S. T. Yu, S. C., Chang, P. C. E. Jorgenson, "Direct Calculation of Detonation with Multi-Step Finite-Rate Chemistry by the Space-Time Conservation Element and Solution Element Method," AIAA Paper 99-3772, AIAA 30th Fluid Dynamics Conference and Exhibit, June 1999, Norfolk, VA.

8. S.T. Yu, S.C. Chang, P.C.E. Jorgenson, S.J. Park, and M.C. Lai, "Basic Equations of Chemically Reactive Flows for Computational Fluid Dynamics," AIAA Paper 98-1051, the 36th Aerospace Sciences Meeting and Exhibit, January 1998, Reno, NV.

9. S.T. Yu, S.C. Chang, P.C.E. Jorgenson, S.J. Park, and M.C. Lai, "Treating Stiff Source Terms in Conservation Laws by the Space-Time Conservation Element and Solution Element Method," the 16th International Conference on Numerical Methods in Fluid Dynamics, June 1998, Arcachon, France.

10. S.T. Yu and S.C. Chang, "Applications of the Space-Time Conservation Element and Solution Element Method to Unsteady Chemically Reacting Flows, AIAA Paper 97-2099, the 13th AIAA CFD Conference, June 1997, Snowmass, Colorado.

11. S.T. Yu and S.C. Chang, "Treatment of Stiff Source Terms in Conservation Laws by the Method of Space-Time Conservation Element and Solution Element," AIAA Paper 97-0435, the 35th AIAA Aerospace Sciences Meeting, January 1997, Reno, NV.

12. S. Gordon and B.J. McBride, "Computer Program for Calculation of Complex Chemical Equilibrium Compositions, Rocket Performance, Incident and Reflected Shocks, and Chapman-Joujuet Detonations," NASA SP-273, March 1976.

13. S. Yungster and K. Radhakrishnan, "Modeling Planar Detonation Wave Propagation Using Detailed Chemistry," AIAA Paper 96-2949, 32nd AIAA/ASME/SAE/ASEE Joint Propulsion Conference, July, 1996, Lake Buena Vista, FL.

14. Y.H. Wu, V. Yang, and K.C. Hsieh, "Simulation of Unsteady Premixed Flame with Detailed Chemistry Kinetics Using the Space-Time Method," AIAA Paper 99-1010, the 37th Aerospace Sciences Meeting and Exhibit, January 1999, Reno, NV.

15. E.S. Oran, T.R. Young, J.P. Boris, and A. Cohen, "Weak and Strong Ignition, I, Numerical Simulations of Shock Tube Experiments," Combustion and Flame, 48 (1982) pp.135-148.

Appendix: Hydrogen/Air reaction mechanism.

Considered species: H_2, O_2, OH, H_2O, H, O, HO_2, H_2O_2, Ar

Reaction rate coefficient in Reference [22], : $K = A*T^m*\exp(-E/R_uT)$

No.	Reaction	A ($(m^3/kmol)^{n-1}/\cdot s$)	m	E/R_u (K)
R1	$H + OH \rightarrow O + H_2$	8.43E+06	1.0	3500
	$O + H_2 \rightarrow H + OH$	1.81E+07	1.0	4480
R2	$H + HO_2 \rightarrow H_2 + O_2$	2.53E+10	0.0	350
	$H_2 + O_2 \rightarrow H + HO_2$	5.48E+10	0.0	29100
R3	$H + HO_2 \rightarrow OH + OH$	2.53E+11	0.0	950
	$OH + OH \rightarrow H + HO_2$	1.20E+10	0.0	20200
R4	$H + HO_2 \rightarrow O + H_2O$	5.00E+10	0.0	500
	$O + H_2O \rightarrow H + HO_2$	1.05E+09	0.45	28400
R5	$H + H_2O_2 \rightarrow HO_2 + H_2$	1.69E+09	0.0	1900
	$HO_2 + H_2 \rightarrow H + H_2O_2$	7.23E+08	0.0	9400
R6	$H + H_2O_2 \rightarrow OH + H_2O$	3.18E+11	0.0	4500
	$OH + H_2O \rightarrow H + H_2O_2$	2.40E+11	0.0	40500
R7	$OH + H_2 \rightarrow H + H_2O$	1.10E+06	1.30	1840
	$H + H_2O \rightarrow OH + H_2$	1.08E+07	1.20	9610
R8	$OH + OH \rightarrow H_2 + O_2$	6.56E+07	0.26	14700
	$H_2 + O_2 \rightarrow OH + OH$	1.69E+10	0.00	24200
R9	$OH + OH \rightarrow O + H_2O$	6.02E+04	1.30	0.00
	$O + H_2O \rightarrow OH + OH$	1.93E+06	1.16	8770
R10	$OH + HO_2 \rightarrow H_2O + O_2$	5.00E+10	0.00	503
	$H_2O + O_2 \rightarrow OH + HO_2$	1.43E+11	0.17	36900
R11	$OH + H_2O_2 \rightarrow HO_2 + H_2O$	1.02E+10	0.00	910
	$HO_2 + H_2O \rightarrow OH + H_2O_2$	2.83E+10	0.00	16500
R12	$HO_2 + H_2 \rightarrow OH + H_2O$	7.23E+08	0.00	9410
	$OH + H_2O \rightarrow HO_2 + H_2$	8.01E+06	0.43	36200
R13	$HO_2 + HO_2 \rightarrow H_2O_2 + O_2$	1.81E+10	0.00	500
	$H_2O_2 + O_2 \rightarrow HO_2 + HO_2$	9.45E+11	-0.38	22000
R14	$O + OH \rightarrow H + O_2$	1.64E+09	0.28	-81.0
	$H + O_2 \rightarrow O + OH$	2.23E+11	0.00	8450
R15	$O + HO_2 \rightarrow OH + O_2$	5.01E+10	0.00	503
	$OH + O2 \rightarrow O + HO_2$	1.32E+10	0.18	28200
R16	$O + H_2O_2 \rightarrow H_2O + O_2$	8.43E+08	0.00	2120
	$H_2O + O_2 \rightarrow O + H_2O_2$	3.43E+07	0.52	44800
R17	$O + H_2O_2 \rightarrow OH + HO_2$	8.43E+08	0.00	2130
	$OH + HO_2 \rightarrow O + H_2O_2$	1.25E+06	0.64	8230
R18	$H + H + M \rightarrow H_2 + M$	6.53E+11	-1.00	0.00
	$H_2 + M \rightarrow H + H + M$	2.23E+11	0.00	48300
R19	$H + OH + M \rightarrow H_2O + M$	2.25E+16	-2.00	0.00
	$H_2O + M \rightarrow H + OH$	3.49E+12	0.00	52900

	+ M			
R20	$H + O_2 + M \rightarrow HO_2 + M$	1.50E+09	0.00	-500
	$HO_2 + M \rightarrow H + O_2 + M$	2.11E+12	0.00	23000
R21	$OH + OH + M \rightarrow H_2O_2 + M$	9.07E+08	0.00	-2550
	$H_2O_2 + M \rightarrow OH + OH + M$	1.20E+14	0.00	22900
R22	$O + H + M \rightarrow OH + M$	3.00E+13	-1.00	0.00
	$OH + M \rightarrow O + H + M$	1.40E+11	0.21	51000
R23	$O + OH + M \rightarrow HO_2 + M$	1.02E+11	0.00	0.00
	$HO_2 + M \rightarrow O + OH + M$	6.62E+16	-0.43	32200
R24	$O + O + M \rightarrow O_2 + M$	1.89E+07	0.00	-900
	$O_2 + M \rightarrow O + O + M$	1.81E+15	-1.00	59400

*n is reaction order

Reaction rate coefficient in Reference [26], : $K = A*T^{m}*\exp(-E/R_uT)$

No.	Reaction	A ($(m^3/kmol)^{n-1}/\cdot s$)	m	E/R_u (K)
R1	$H_2 + O_2 \Leftrightarrow HO_2 + H$	1.00E+11	0.00	28197.38
R2	$H + O_2 \Leftrightarrow OH + O$	2.60E+11	0.00	8459.21
R3	$H_2 + O \Leftrightarrow OH + H$	1.80E+07	1.00	4481.37
R4	$H_2 + OH \Leftrightarrow H + H_2O$	2.20E+10	0.00	2593.15
R5	$OH + OH \Leftrightarrow O + H_2O$	6.30E+09	0.00	548.84
R6*	$H + OH + M \Leftrightarrow H_2O + M$	2.20E+16	-2.00	0.00
R7*	$H + H + M \Leftrightarrow H_2 + M$	6.40E+11	-1.00	0.00
R8*	$H + O + M \Leftrightarrow OH + M$	6.00E+10	-0.60	0.00
R9*	$H + O_2 + M \Leftrightarrow HO_2 + M$	2.10E+09	0.00	-503.52
R10	$O + O + M \Leftrightarrow O_2 + M$	6.00E+07	0.00	-906.34
R11	$HO_2 + H \Leftrightarrow OH + OH$	1.40E+11	0.0	543.81
R12	$HO_2 + H \Leftrightarrow H_2O + O$	1.00E+10	0.0	543.81
R13	$HO_2 + O \Leftrightarrow O_2 + OH$	1.50E+10	0.00	478.35
R14	$HO_2 + OH \Leftrightarrow H_2O + O_2$	8.00E+09	0.00	0.00
R15	$HO_2 + HO_2 \Leftrightarrow H_2O_2 + O_2$	2.00E+09	0.00	0.00
R16	$H + H_2O_2 \Leftrightarrow H_2 + HO_2$	1.40E+09	0.0	1812.69
R17	$O + H_2O_2 \Leftrightarrow OH + HO_2$	1.40E+10	0.00	3222.56
R18	$OH + H_2O_2 \Leftrightarrow HO_2 + H_2O$	6.10E+09	0.00	720.04
R19*	$H_2O_2 + M \Leftrightarrow OH + OH + M$	1.20E+14	0.00	22910.37

*Third body efficients:
Reaction 6: H_2O =6.0, Reaction 7: H_2O=6.0
Reaction 8: H_2O =5.0, Reaction 9: H_2O=16.0, H_2=2.0
Reaction 19: H_2O=15.0
The backward reaction rate was calculated by Gibbs free energy using Equation (2.17) and (2.20).